

Article

Design and SAR Analysis of a Dual Band Wearable Antenna for WLAN Applications

Ashfaq Ahmad ¹, Farooq Faisal ², Sadiq Ullah ³ and Dong-You Choi ^{1,*}

- ¹ Communication and Wave Propagation Laboratory, Department of Information and Communication Engineering, Chosun University, Gwangju 61452, Korea
- ² National Institute of Scientific Research (INRS), University of Quebec, Montreal, QC H5A 1C6, Canada
- ³ Department of Telecommunication Engineering, University of Engineering and Technology, Mardan 23200, Pakistan
- * Correspondence: dychoi@chosun.ac.kr

Abstract: This paper presents the design of three types of dual band (2.5 & 5.2 GHz) wearable microstrip patch antennas. The first one is based on a conventional ground plane, whereas the other two antennas are based on two different types of two-dimensional electromagnetic band gap (EBG) structures. The design of these two different dual-band EBG structures using wearable substrates incorporates several factors in order to improve the performance of the proposed conventional ground plane (dual band) wearable antenna. The second EBG with plus-shaped slots is about 22.7% more compact in size relative to the designed mushroom-like EBG. Subsequently, we have demonstrated that the mushroom-like EBG and the EBG with plus-shaped slots improve the bandwidth by 5.2 MHz and 7.9 MHz at lower resonance frequencies and by 33.6 MHz and 16.7 MHz at higher resonance frequencies, respectively. Furthermore, improvements in gain of 4.33% and 16.5% at a frequency of 2.5 GHz and improvements in gain of 30.43% and 4.57% at 5.2 GHz have been achieved by using the mushroom-like EBG and EBG with plus-shaped slots, respectively. The operation of the conventional ground plane antenna is investigated under different bending conditions, such as wrapped around different rounded body parts. The proposed conventional ground plane antenna is placed over a three-layered (flat body phantom (chest)) and four-layered (rounded body parts) tissue models, and a thorough SAR analysis has been performed. It is concluded that the proposed antenna reduces SAR effects (<2 W/kg) on the human body, thereby making it useful for numerous critical wearable applications.

Keywords: wearable antenna; electromagnetic band gap (EBG); wireless body area network (WBAN); SAR analysis; on/off-body simulations; CST MWS software



Citation: Ahmad, A.; Faisal, F.; Ullah, S.; Choi, D.-Y. Design and SAR Analysis of a Dual Band Wearable Antenna for WLAN Applications. *Appl. Sci.* **2022**, *12*, 9218. <https://doi.org/10.3390/app12189218>

Academic Editors: Bhanu Shrestha, Seongsoo Cho and Changho Seo

Received: 28 July 2022

Accepted: 12 September 2022

Published: 14 September 2022

Publisher's Note: MDPI stays neutral with regard to jurisdictional claims in published maps and institutional affiliations.



Copyright: © 2022 by the authors. Licensee MDPI, Basel, Switzerland. This article is an open access article distributed under the terms and conditions of the Creative Commons Attribution (CC BY) license (<https://creativecommons.org/licenses/by/4.0/>).

1. Introduction

Wearable systems provide an extension in the classical concept of wearable apparel, which is used for the protection of the body from environmental effects. These systems have introduced new services and need to be completely integrable into the wearable apparel without affecting its comfortability and wearability. A wearable antenna is the main component in a wearable system and serves as a crucial bridge between the external electronic devices and the on-body electronic circuitry [1]. These antenna-based systems are being utilized for security, rescue, sports, entertainment and many other applications [2]. Therefore, they are expected to exhibit resilience to the harsh environment and have a small size. Antenna miniaturization is often achieved by the reduction of the ground plane [3]. However, a reduced ground plane results in spurious currents flowing in the ground plane, which can affect the radiation characteristics of that antenna. Some other miniaturization techniques are also used for antenna size reduction, such as loading lumped components, creating slots [4] and bends, and using short circuits and spiral-shaped radiators [5], among many other techniques. However, patch antennas, because of their peculiar properties, are

always favorable for wearable applications [6]. The radiation pattern of a patch antenna is perpendicular to the antenna plane, which is why, in terms of low specific absorption rate (SAR), patch antennas are the best candidates for these applications. Furthermore, the full ground plane, which is a component of a patch antenna, is beneficial in preventing the wearer's body from unwanted radiation [7], and this further helps reduce the SAR value.

Whenever an antenna is installed on a wearer's body, its side and back radiation lobes penetrate into the user's body, thereby being absorbed. Absorption of these lobes or waves produce hot spots on the human body, and destruction of tissues may occur [8,9]. The specific absorption rate (SAR) defined in Equation (1) is the value formulated to calculate the absorption of electromagnetic waves by human tissue:

$$\text{SAR} = \frac{\sigma E^2}{\rho} \text{ (W/kg)} \quad (1)$$

where E is the root-mean-square electric field induced in the tissue (V/m), ρ is the tissue density (kg/m^3) and σ is the tissue electrical conductivity (s/m), and its value dictates quantity of maximum exposure to the electromagnetic fields. Beginning in the year 1990, the SAR value of the interaction of an antenna with the human body received tremendous attention [10,11] because of the huge increase in wireless body area network (WBAN) applications. The SAR value should not exceed the recommended exposure thresholds, and it should remain within a predefined SAR limit. Therefore, different techniques [12,13] were used by researchers to bring the SAR value into the desired limit. The electromagnetic band-gap (EBG) acts as a shield and reduces the SAR value [14,15] by efficiently radiating the side and back radiation lobes in the forward direction to protect the human body. It has been shown in some publications [16] that a ferrite sheet also acts as a protective shield and provides stability in terms of resonant frequencies, irrespective of the antenna position on the body. It therefore can be used as an alternative to EBG for SAR reduction.

In most cases, the antenna performance is degraded when it is in proximity to the wearer's body or when it acquires a bend [17]. This degradation in performance is due to the permittivity and conductivity of human tissues. Besides the effects due to conductivity and permittivity of tissues, bending may produce a change in the effective electrical length of antenna or mismatch the impedance. Consequently, a shift in the resonance frequency or decrease/increase in the return loss may occur [18]. Therefore, an evaluation of the different parameters of a wearable antenna on a body and in different bending conditions is required to be explored. High impedance surfaces or EBG structures are used to minimize this degradation in performance [14]. EBG structures are artificial materials used as a ground plane for antennas. These structures enhance the overall performance of an antenna by providing in-phase reflection and surface wave suppression [19–22]. Another aspect of EBG can be found in array antennas. Mutual coupling is a severe problem in array antennas or multiple antenna systems [23,24]. This problem of mutual coupling between multiple antenna elements can be overcome by utilizing EBG [25,26]. Instead of EBG, the same objective can be achieved by using defected ground structures (DGS) [27]. However, in some cases, as in [28], the gain of the array antenna may be significantly reduced by using DGS. Therefore, EBG is a better choice compared to DGS.

In most of the work in literature, only flat antenna conditions are usually considered for the antenna performance [29] and SAR measurements [30,31]. However, due to the flexibility of wearable antennas, it is not possible for these antennas to maintain their flat conditions all the time on a wearer's body. Moreover, the SAR value is a function of the bending radius of a specified body organ [32]; the smaller the bending radius, the worse the SAR value. Furthermore, crumpling and bending an antenna may reduce its performance, as reported in [33]. Therefore, in this paper, we provide a comprehensive SAR analysis as well as the impact of other antenna parameters on both flat and bending conditions. In addition, we consider antenna bending conditions based on various wearable antenna radii sizes specified on the basis of the corresponding human arms and legs on which they are wrapped.

In this work, a very compact size dual band wearable microstrip patch antenna operating at 2.5 and 5.196 GHz is designed. In order to improve the performance of antenna in terms of directivity, gain and bandwidth, two types of EBG ground planes were designed for the proposed conventional antenna. The antenna is low profile and conformable and is composed of a textile material called polyethylene foam, having a relative permittivity of 1.05. The proposed antenna is bent around human legs and arms of different radii, and its operation is studied under various bent conditions. For the on-body simulation, two types of body phantoms are modeled. The first one is a flat body phantom (used for the chest) consisting of three layers, whereas the second one is a cylindrical body phantom (used for the arms and legs) consisting of four different layers. The proposed antenna is placed on the flat body phantom as well as bent around arms (of different radii) and legs, and its SAR analysis is carried out. We use CST MWS software for all the simulations and analysis in this work.

The rest of the paper is organized into the following sections. Section 2 provides our design methodology using various approaches. In Section 3, we present the human phantom modeling approach and describe our simulation results based on off-body and on-body analyses. Furthermore, we thoroughly discuss the impact of various antenna positions. In Section 4, we conclude the paper and discuss some open questions.

2. Design Methodology

2.1. Conventional Approach

All the designs and simulations in this project were carried out in CST MWS software with a frequency range of 2 to 5.5 GHz. The geometrical model of the proposed dual band wearable patch antenna is shown in Figure 1. The 3 mm thicker substrate having a compact size of 68 mm × 73 mm was made of polyethylene foam with a relative permittivity of 1.05 [34]. The overall size of the radiating patch was 44.75 mm × 47 mm. A 50 Ω microstrip feed line was used in the design of the proposed dual band textile antenna. The dimensions of the proposed dual band textile antenna were obtained by using the theory of transmission lines [35].

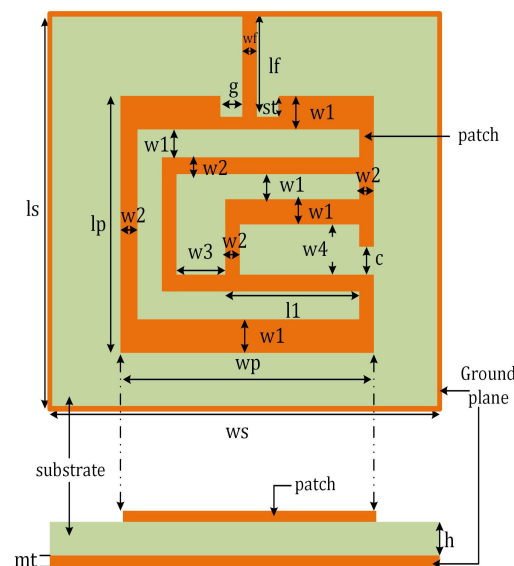


Figure 1. Geometrical model of the proposed dual band microstrip patch antenna.

Table 1 presents the optimized values of the parameters mentioned in Figure 1.

Table 1. List of simulation parameters along with their optimized values.

Parameter	Description	Value (mm)	Parameter	Description	Value (mm)
ls	Substrate or ground plane length	68	g	Gap at sides of the feed line	5
ws	Substrate or ground plane width	73	st	Depth of the gap with the feed line	3.5
lp	Patch length	44.75	c	Right side cut length	10
wp	Patch width	47	w1	Width of the upper or centered or bottom strip	5
h	Substrate thickness	3	w2	Width of the right or left side strip	3.5
mt	Patch or ground plane thickness	0.03	w3	Width of the p shaped cut	9
lf	Microstrip feed line length	15.125	w4	Width of the I shaped cut	12
wf	Microstrip feed line width	5	l1	Length of the I shaped cut	26

2.2. Metamaterial Based Approach

Metamaterials are artificially-designed materials that are used as a ground plane to enhance the performance of an antenna. These materials offer suppression of surface waves at intended frequency bands, thereby offering improvements in efficiency, gain, directivity and other parameters of an antenna. The design of two different unit cells of the two different EBG structures to be employed as a ground plane for the designed dual band wearable antenna is outlined in the section below.

2.2.1. Dual Band EBG Unit Cells

This section summarizes the design and analysis of two different unit cells of the two different EBG structures for the desired frequency bands (2.5 GHz and 5.196 GHz). Polyethylene with a thickness of 3 mm was utilized as a substrate material in the design of these two EBG structures. For the unit cell, the resonant frequency depends on the effective capacitance (C) and inductance (L) of the unit cell, i.e.,

$$f_r = \frac{1}{2\pi\sqrt{LC}} \quad (2)$$

$$C = \frac{w\epsilon_0(1 + \epsilon_r)}{\pi} \cosh^{-1} \frac{a}{g} \quad (3)$$

$$L = \mu_0 h \quad (4)$$

where μ_0 and ϵ_0 are the free space permeability and permittivity, respectively. Figure 2 presents the design of the two dual band EBG unit cells. The first one is the conventional mushroom-like EBG unit cell. It is a square shape with overall dimensions of 32.5 mm \times 32.5 mm. The radius of the via is 1.5 mm. The second unit cell is different from the conventional mushroom-like EBG unit cell. A plus-shaped slot is created in the unit cell. The creation of slots increases the capacitance and thus makes the proposed unit cell more compact in size as compared to the conventional mushroom-like EBG unit cell [36]. The second EBG unit cell with a plus-shaped slot has a total size of 26.5 mm \times 26.5 mm. The second EBG unit cell is about 18.46% more compact in size as compared to the conventional mushroom-like EBG unit cell. The width and length of the plus-shaped slot in the second EBG unit cell are 3 mm and 13 mm, respectively.

The in-phase reflection of the proposed dual-band EBG unit cells are shown in Figure 3. It is observed that in the case of each EBG unit cell, the in-phase response is shown on the desired resonances (2.5 GHz and 5.2 GHz).

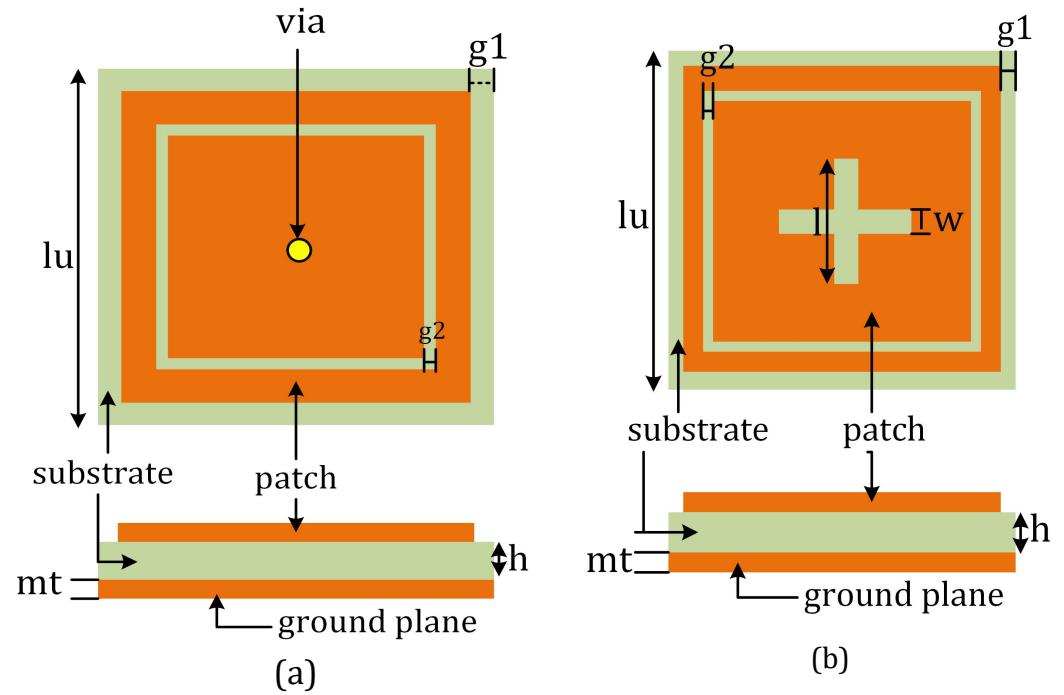


Figure 2. EBG unit cells. (a) Mushroom-like EBG unit cell. (b) Unit cell with plus-shaped slots.

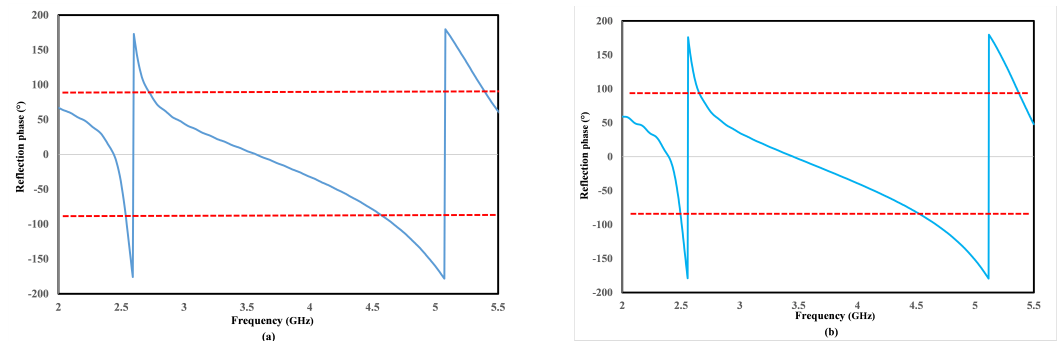


Figure 3. In-phase reflection of EBG unit cells. (a) Mushroom-like unit cell. (b) Unit cell with plus-shaped slots.

Table 2 presents the values of the parameters of the unit cells given in Figure 2.

Table 2. Summary of the EBG unit cells dimensions.

Type	lu (mm)	g1 (mm)	g2 (mm)	h (mm)	r (mm)	l (mm)	w (mm)	Periodicity
Mushroom-like EBG unit cell	32.5	2	1.5	3	1.5			32.5
Plus-shaped slot EBG unit cell	26.5	0.5	1.1	3		13	3	26.5

Table 2 shows that the EBG unit cell with the plus-shaped slot is more compact than the mushroom-like EBG unit cell.

2.2.2. Electromagnetic Band-Gap Array

Surface wave suppression is one of the most important properties of EBG structures. Suppression of surface waves improves the gain, directivity and other parameters of the antenna, while it minimizes side and back lobes [37]. The scattering parameters of the

two EBG surfaces are achieved by the use of two port transmission line techniques, as depicted in Figure 4. Out of the two ports, the one to the left side is supposed as the source of excitation, and the other to the right side is supposed as a matched load. The mushroom-like EBG array has a total size of 176.5 mm × 176.5 mm, while the second EBG array with plus-shaped slots is 136 mm × 136 mm.

The reflection and transmission coefficients of the two EBG structures are depicted in Figure 5. It shows that in the case of each EBG, the S21 is lower than −15 dB at both frequencies (2.5 GHz and 5.196 GHz). Therefore, both EBG structures have the ability to suppress surface waves in the desired frequency bands (2.5 GHz and 5.196 GHz). However, the second EBG structure with plus-shaped slots is about 22.94% more compact than the conventional mushroom-like EBG array.

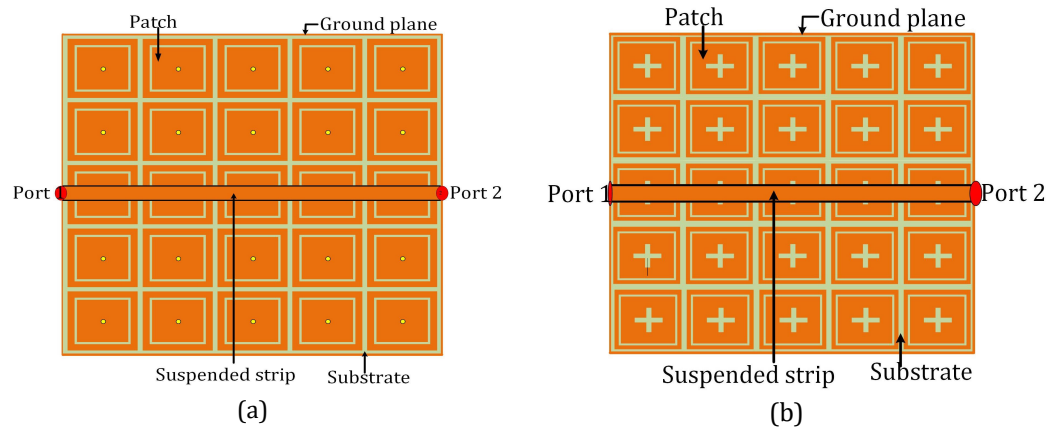


Figure 4. A 5×5 array of (a) the mushroom EBG and (b) the EBG with plus-shaped slots with suspended strips.

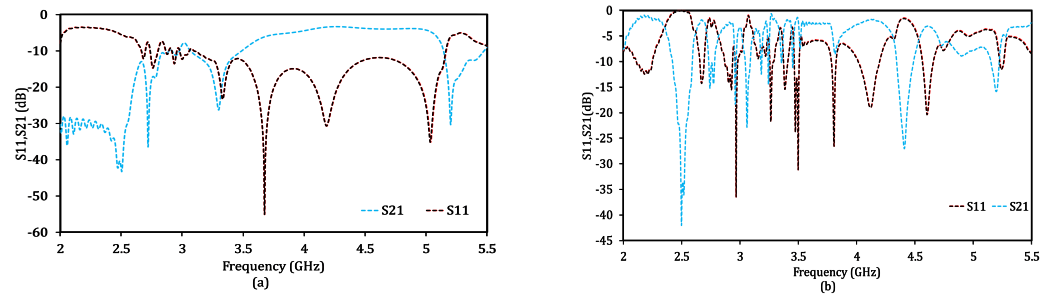


Figure 5. Reflection and transmission coefficients of 5 × 5 EBG array. (a) Mushroom-like EBG unit; (b) EBG with plus-shaped slots.

2.3. EBG-Based Antenna

The proposed dual band textile antenna was placed over two different 5 × 5 EBG ground planes as shown in Figure 6. In the case of the mushroom-like EBG’s ground plane, the overall dimension of the antenna was 176.5 mm × 176.5 mm, whereas, in the case of the EBG ground plane with plus-shaped slots was 136 mm × 136 mm.

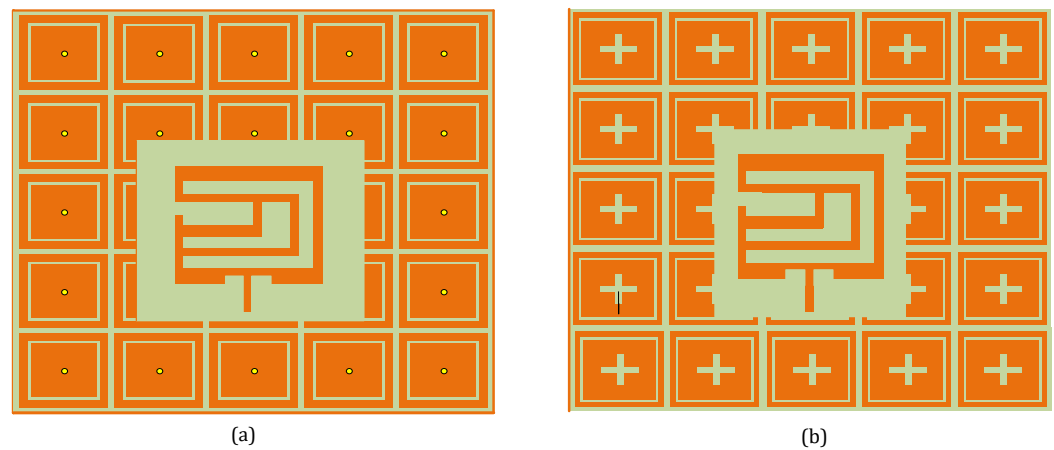


Figure 6. Antenna over EBG ground planes. (a) Mushroom-like EBG; (b) EBG with plus-shaped slots.

This means that the antenna with second ground plane is about 22.94% more compact in size than the mushroom-like EBG-based antenna.

2.4. Human Phantom Modeling

For the on-body analysis of the proposed dual band wearable antenna, two body parts were modeled in CST MWS. The first one was a flat homogeneous phantom (chest) with three layers used to model muscle, fat and skin. Similarly, the second one was a heterogeneous cylindrical phantom with four layers to model bone, muscle, fat and skin. The flat body phantom had overall dimensions of 160 mm \times 180 mm \times 53 mm, as shown in Figure 7. The thickness of the muscle layer was 50 mm, while the thickness of the fat layer was 2 mm and the skin was 1 mm.

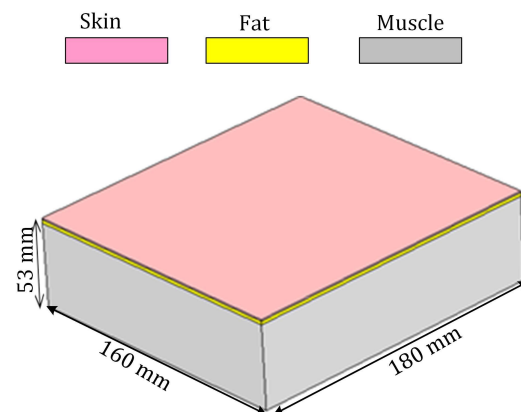


Figure 7. Overall flat body phantom used for modeling the typical human chest.

In the second case, three heterogeneous cylindrical models of body parts were designed, and the proposed dual band antenna was bent over them, as shown in Figure 8. The first one was a leg having a total radius of 70 mm. The second one was a healthy arm having a 60 mm radius, and the third one, which models the worst condition among all, was a child's arm having a 40 mm radius.

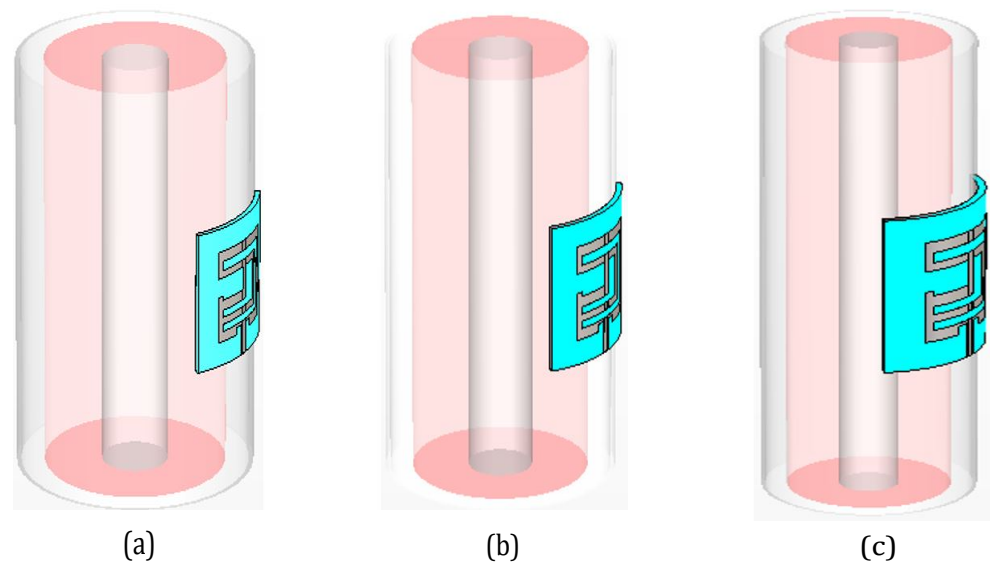


Figure 8. Antenna wrapped around four-layered body parts. (a) Leg of radius 70 mm; (b) arm of radius 60 mm; (c) arm of radius 40 mm.

The average typical electromagnetic properties for the human tissues (bone, muscle, fat and skin) at 2.5 GHz and 5.2 GHz are taken from [38] and are given in Table 3.

Table 3. Average EM properties of human tissues at 2.5 GHz and 5.2 GHz.

Tissue	Conductivity (2.5 GHz), S/m	$\epsilon_r/2.5$ GHz	Conductivity (5.2 GHz), S/m	$\epsilon_r/5.2$ GHz
Bone	0.38459	11.41	1.0101	9.946
Muscle	1.705	52.79	4.2669	49.278
Fat	0.10235	5.28	0.2547	5.0104
Skin	1.4407	38.06	3.2185	35.61

3. Results

3.1. Off-Body Analysis

3.1.1. Conventional Antenna

The proposed dual-band wearable antenna operating at 2.5 GHz and 5.2 GHz was designed in CST MWS software with a frequency range of 2 to 5.5 GHz, as shown in Figure 1. Figure 9 shows the return loss of the designed dual band antenna. The resonance frequencies were 2.5 and 5.2 GHz with an input impedance bandwidth of 23.8 and 60.4 MHz, respectively. The proposed antenna had a return loss of -24.975 and -28.234 at 2.5 and 5.5 GHz, respectively.

Figure 10 shows that the proposed antenna is very precisely matched at both resonance frequencies with a voltage standing wave ratio (VSWR < 1.119).

The directivity and gain patterns of the designed conventional dual band antenna at 2.5 and 5.2 GHz are shown in Figures 11 and 12, respectively. The maximum directivities at 2.5 and 5.2 GHz are 8.39 and 9.01 dB, respectively. The 3dB angular widths at 2.5 and 5.2 GHz are 83.4 and 76.9 degrees, respectively. The maximum gains at 2.5 and 5.2 GHz are 8.08 and 8.74 dBi, respectively. A small amount of disturbance is observed in the patterns at the higher resonance frequency. The second reason for this disturbance is the compact size of the proposed antenna. The miniaturization of an antenna is always a matter of compromise between antenna radiation characteristics and its size. Therefore, various slots

have been created in the designed dual band antenna to bring it to a very compact size of $68 \times 73 \text{ mm}^2$.

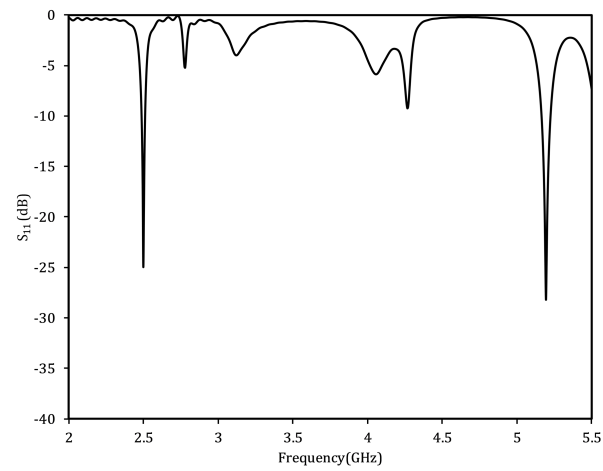


Figure 9. Reflection coefficient of conventional dual band antenna.

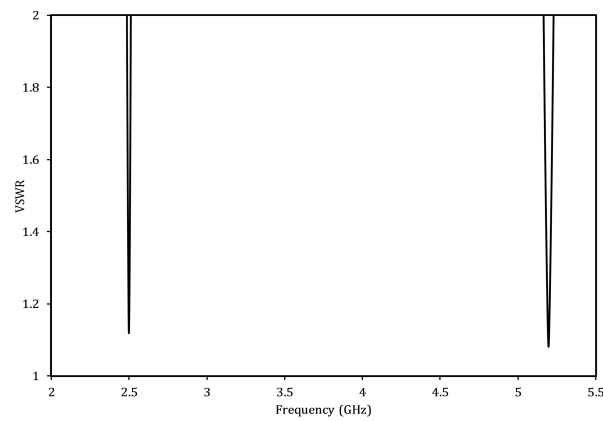


Figure 10. VSWR of conventional dual band antenna.

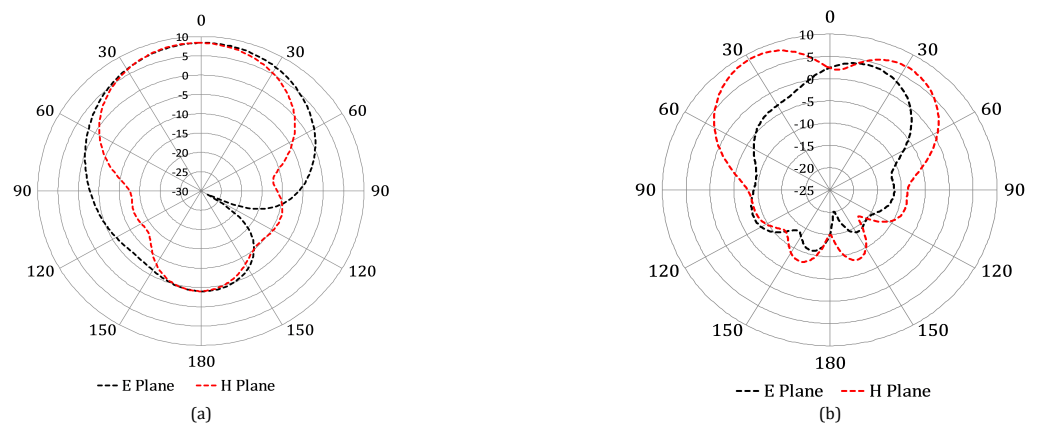


Figure 11. Directivity patterns of conventional dual band antenna at (a) 2.5 GHz (b) 5.2 GHz.

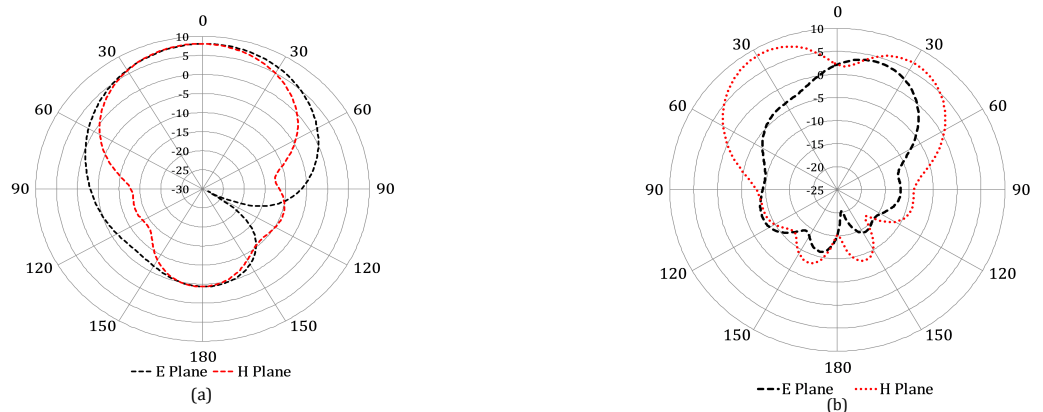


Figure 12. Gain patterns of conventional dual band antenna at (a) 2.5 GHz and (b) 5.2 GHz.

The distribution of surface currents in the conventional wearable antenna at 2.5 and 5.2 GHz is shown in Figure 13, which clearly shows the resonant lengths.

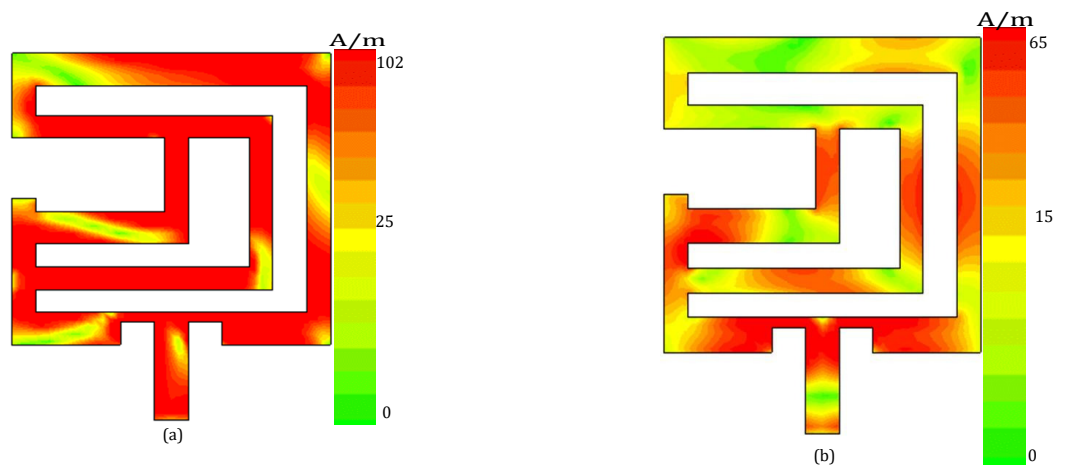


Figure 13. Distribution of surface currents of the conventional dual band antenna at (a) 2.5 GHz and (b) 5.2 GHz.

3.1.2. Metamaterial-Based Antenna

To improve the performance of the designed conventional dual band antenna, two different types of EBG ground planes have been designed in CST software, as shown in Figure 3. Subsequently, these EBG surfaces have been employed as a ground plane for the proposed dual band wearable antenna, as shown in Figure 6, and an analysis on the basis of a performance comparison is presented below.

Figure 14 shows the comparison of the return loss of the conventional dual band wearable antenna with that of the two EBG-based ground plane antennas.

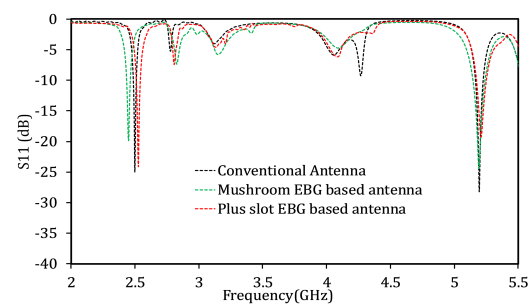


Figure 14. Return loss without EBG and with EBG ground planes.

With the help of the mushroom-like EBG ground plane, a 5.2 and 33.6 MHz improvement in bandwidth has been achieved for the lower and upper frequency bands, respectively. By using the EBG with plus-shaped slots as the ground plane for the proposed antenna, a 7.9 and 16.7 MHz improvement has been achieved in the bandwidth for the 2.5 and 5.2 GHz bands, respectively. A small amount of reduction in return loss has been observed for both EBG ground planes. Moreover, for the lower frequency band, a certain amount of shift to the left side for the mushroom-like EBG ground plane and to the right side for the EBG with plus-shaped slots has been observed. This shift in the resonance frequencies has also been observed in [36,39] when the antenna is employed on a metamaterial-based ground plane.

The directivity and gain patterns without and with EBG ground planes at 2.5 and 5.2 GHz are shown in Figures 15 and 16. An increase of approximately 1.8% and 28.7% in directivity for the lower and upper frequency bands, respectively, has been achieved by the help of the mushroom-like EBG ground plane. By using the EBG with plus-shaped slots, a 15.13% improvement in directivity for the lower frequency band and a 3.55% improvement in that for the higher frequency band have been observed. Similarly, the mushroom-like EBG and EBG with plus-shaped slots show 4.33% and 16.70% improvements in gain for the lower frequency band, respectively, and 30.43% and 4.57% increases in gain for the upper frequency band, respectively. Furthermore, a reduction in side and back lobes is clearly observed in the case of both EBG ground planes. Apart from the directivity and gain, the radiation and total efficiency increase sufficiently for both the resonance bands in the case of both EBG ground planes.

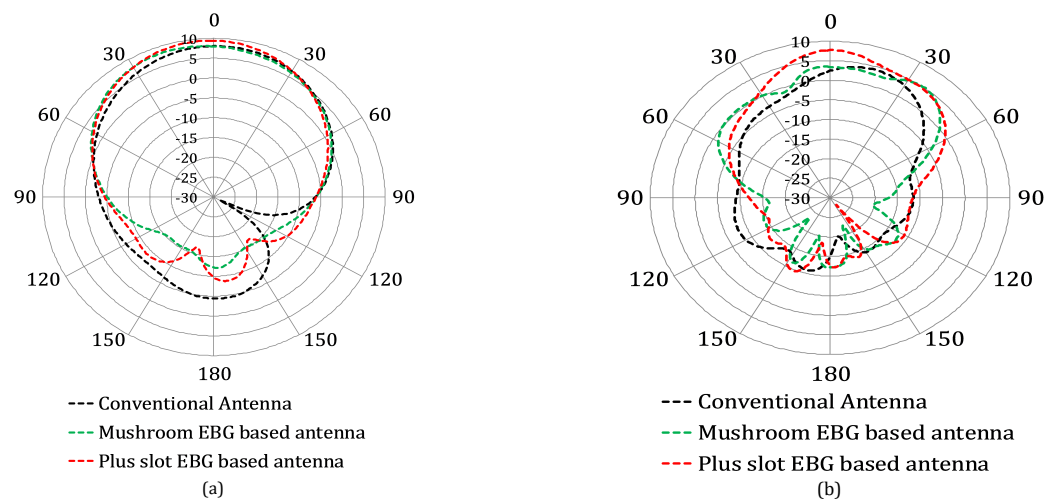


Figure 15. Directivity patterns with and without EBG ground planes at (a) 2.5 GHz and (b) 5.2 GHz.

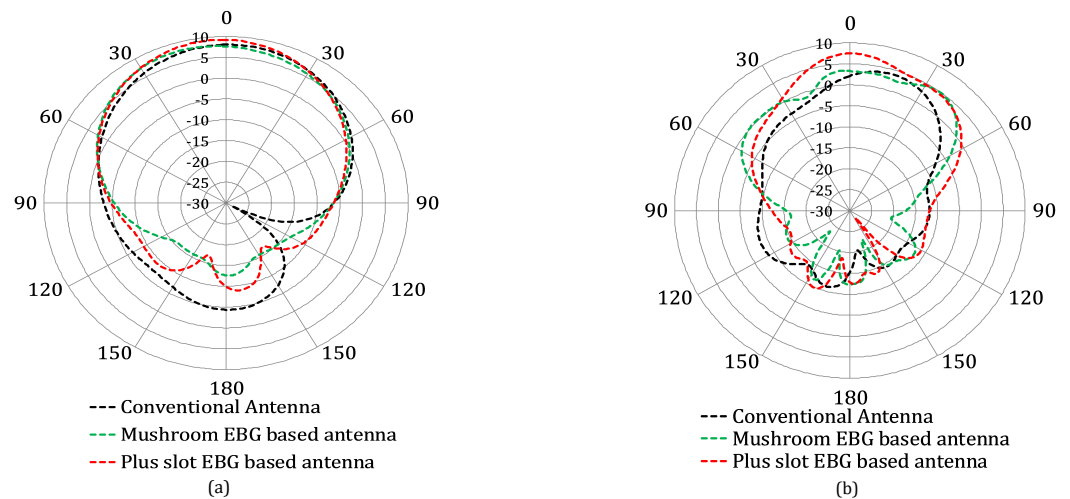


Figure 16. Gain patterns without and with EBG ground planes at (a) 2.5 GHz and (b) 5.2 GHz.

Table 4 summarizes the performance comparison of the conventional dual band antenna without and with EBG ground planes.

Table 4. Performance comparison of proposed dual band antennas with and without EBG ground planes.

Parameter	Conventional Dual Band Antenna		Mushroom-like EBG-Based Antenna		EBG with Plus-Shaped Slots-Based Antenna	
	2.5	5.196	2.452	5.192	2.528	5.208
Frequency (GHz)	2.5	5.196	2.452	5.192	2.528	5.208
Bandwidth (MHz)	23.8	60.4	29	94	31.7	77.1
Return loss (dB)	−24.975	−28.234	−19.82	−24.41	−24.06	−19.25
Directivity (dB)	8.39	9.01	8.55	11.6	9.66	9.33
Gain (dBi)	8.08	8.74	8.43	11.4	9.43	9.14
Radiation Efficiency (%age)	93.06	93.94	97.43	96.17	94.89	95.71
Total efficiency (%age)	92.76	93.80	96.41	95.82	94.52	94.58
Angular width (Deg)	83.4	76.9	80.2	99.4	62.8	70.2

3.1.3. Conventional Antenna in Different Free Space Bending Conditions

The primary utilization of wearable antennas is their usage in on-body health or sports equipment or in security gadgets. All these applications are wearable in nature, and hence, it is impossible to maintain a regular flat antenna condition all the time when these gadgets are worn on the wearer’s body. Consequently, the antenna bending phenomenon occurs during its regular operation, which can adversely affect the performance of the corresponding system of gadget installed with the antenna. For this reason, a thorough analysis of a wearable antenna in various bending conditions can result in improved designs and better results in future wearable systems. Therefore, we used the conventional dual band wearable antenna as given in Figure 1 and bent it around different body parts as shown in Figure 8. In this work, we analyzed our proposed conventional antenna by evaluating its various bending conditions on the basis of its return loss and radiation characteristics. We describe our analysis of various results of the antenna system below.

Figure 17 illustrates the effects on the return loss of the conventional dual band wearable antenna due to bending around a leg with a radius of 70 mm, a healthy arm with a radius of 60 mm, and the worst case, which is a child’s arm with a radius of 40 mm. It is worth noticing that irrespective of the bending radii, the return loss result of the antenna is

stable when bent on these body parts. The return loss is improved by about 15.16 dB at 2.5 GHz for bending around the radius of a child’s arm (40 mm). Similarly it is improved by about 5.68 dB at 5.2 GHz for bending around a leg of radius 70 mm. It is clear from Figure 17 that the bending radii have no prominent effects on the return loss of the proposed dual band wearable antenna.

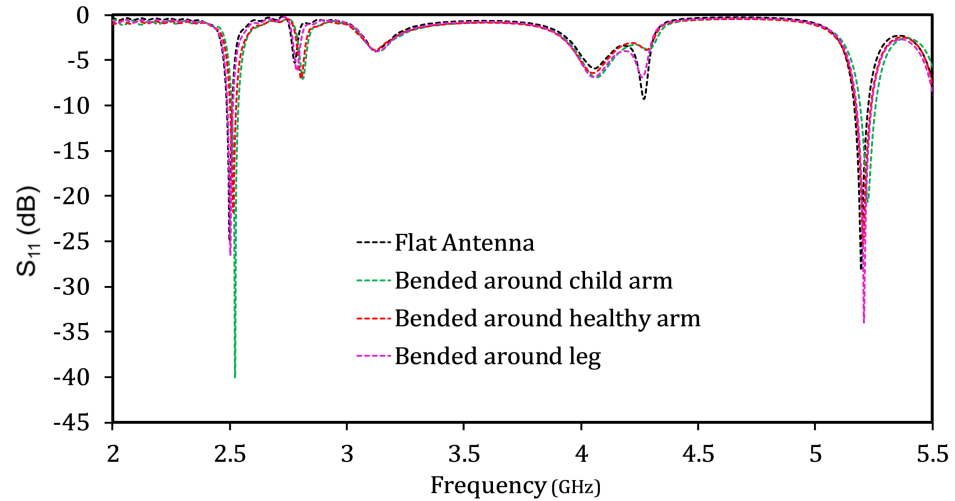


Figure 17. Off-body reflection coefficient of the conventional dual band antenna.

Figures 18 and 19 portray the effects on the directivity and gain patterns, respectively, at the desired resonance frequencies when the proposed conventional dual band patch antenna is bent around body parts of different radii. It is worth mentioning that a very small amount of reduction in directivity and gain for the lower frequency band is observed as the bending radius decreases. However, there is no prominent effect of the bending on the radiation characteristics of the conventional patch antenna, and its overall performance remains stable in terms of return loss and radiation patterns.

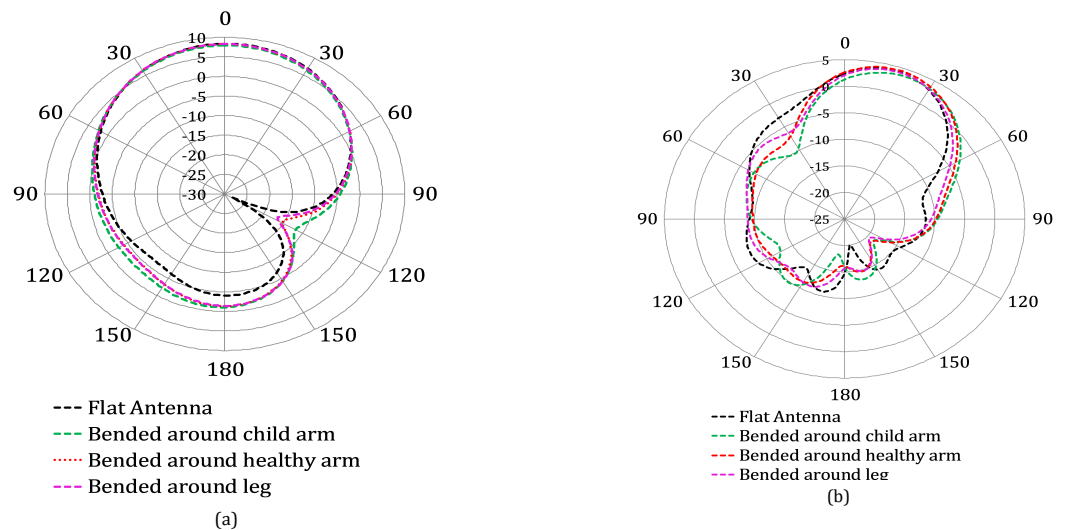


Figure 18. Off-body directivity patterns of the conventional dual band antenna at (a) 2.5 GHz and (b) 5.2 GHz.

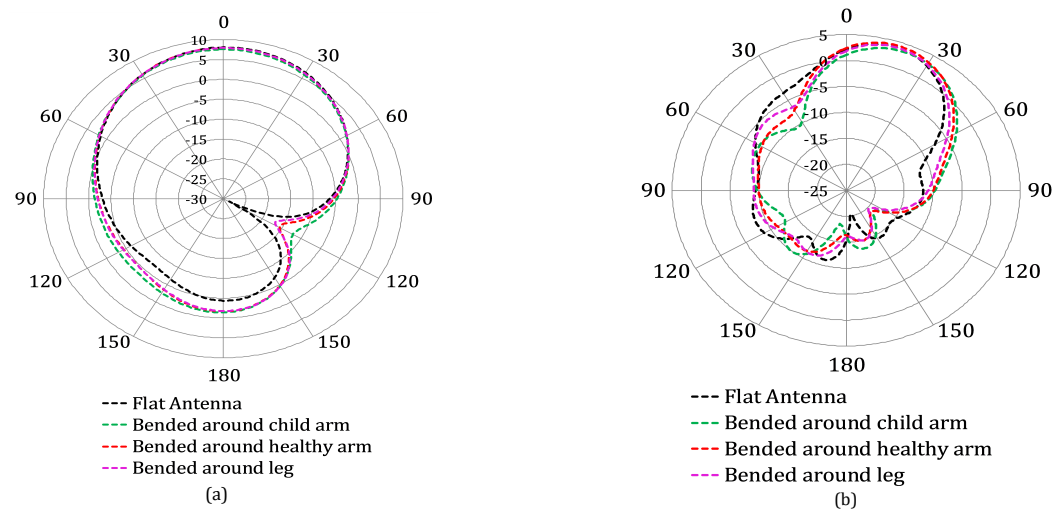


Figure 19. Off-body gain patterns of the conventional dual band antenna at (a) 2.5 GHz and (b) 5.2 GHz.

3.2. On-Body Analysis

In this section, the proposed dual band conventional antenna is placed over human body and an analysis is conducted on the basis of the return loss, radiation patterns and specific absorption rate (SAR) values.

3.2.1. Return Loss

Figure 20 presents the return loss comparison of the proposed conventional antenna without a body, with the flat body phantom, and bent around rounded body parts (leg and arms). Both resonance frequencies increase as the antenna is placed over the body parts. This is due to the permittivity and conductivity of human tissues. Moreover, the shift in the resonance frequencies towards the right side increases as the bending radius decreases. This is due to the fact that the effective resonant length of the antenna depends on the bending radii. The smaller the bending radii, the greater the reduction in the effective length of the antenna, and therefore, shifting of the resonant frequency towards higher frequencies is observed [40]. However, in general, it can be observed that the proposed antenna is tuned all the time, irrespective of the different environmental conditions.

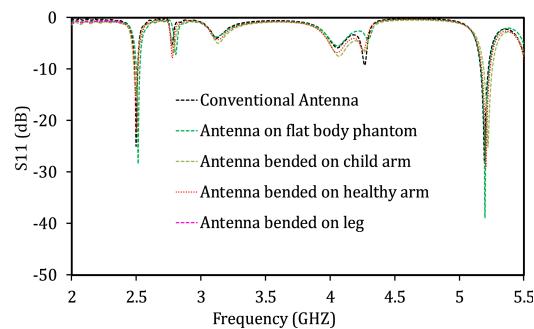


Figure 20. On-body return loss of conventional dual band antenna.

3.2.2. Directivity and Gain Patterns

The directivity and gain patterns of the designed conventional antenna, without a body and when mounted on different body parts, are shown in Figures 21 and 22, respectively. These figures demonstrate that among all conditions, antenna to be placed over a flat body phantom is the most suitable choice in terms of side and back lobes. For rounded body parts, the side and back lobes decrease dramatically as the bending radius increases,

and the radiation patterns approach that of the flat body condition. Table 5 presents a comparison on the basis of maximum gain and directivity between the conventional antenna without a body and the antenna with a child’s arm with a radius of 40 mm (worst case). A small amount of reduction at the lower resonance frequencies has been observed in both the maximum gain and directivity when the designed antenna is worn on a child arm (worst case).

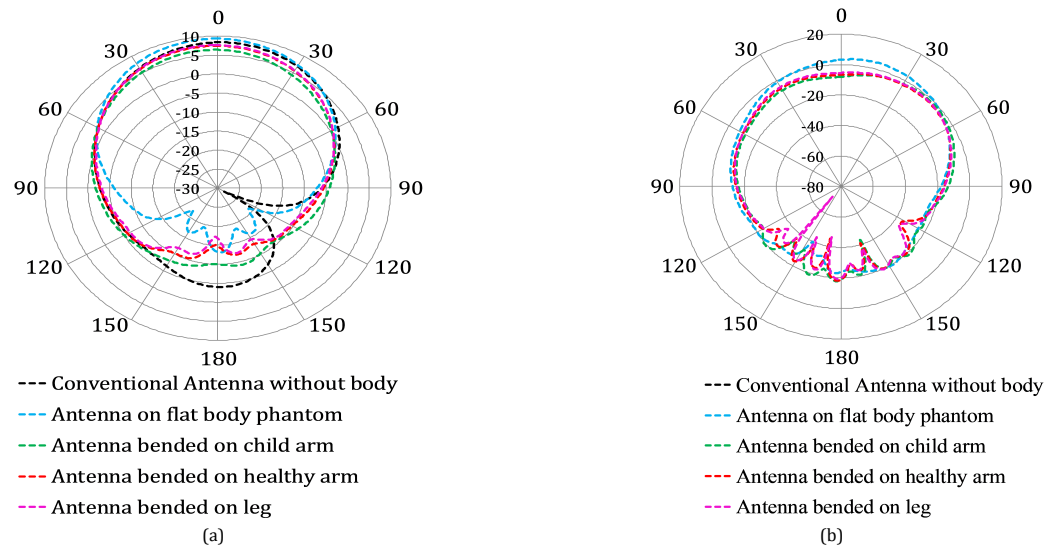


Figure 21. On-body directivity patterns at (a) 2.5 GHz and (b) 5.2 GHz.

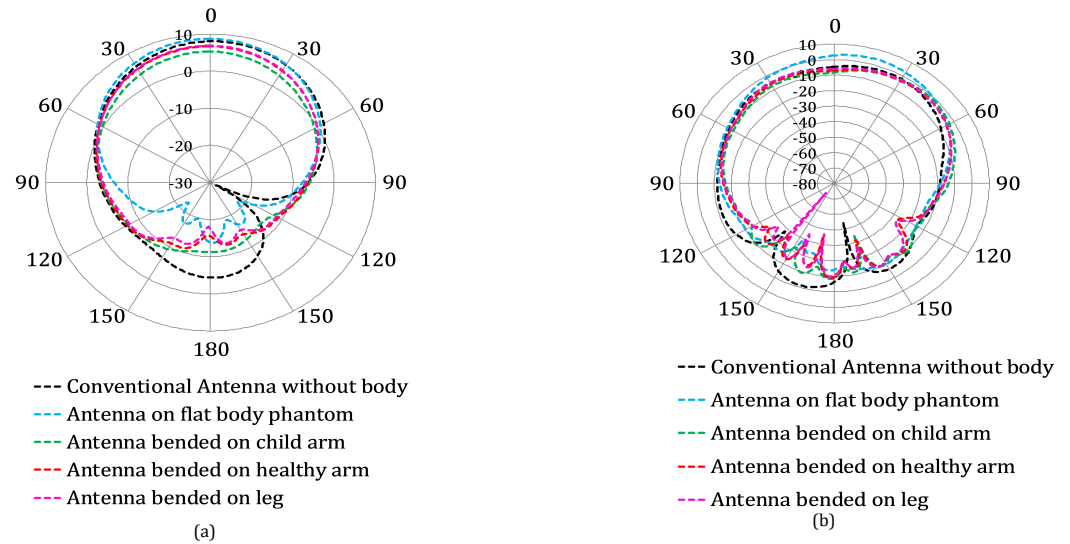


Figure 22. On-body gain patterns at (a) 2.5 GHz and (b) 5.2 GHz.

3.3. Specific Absorption Rate (SAR) Analysis of Conventional Dual Band Antenna

Whenever an antenna is installed on a human body, a part of the electromagnetic waves (EMW) radiated by that antenna is absorbed into the human body in the form of side and back lobes. The specific absorption rate (SAR) is the term used for the evaluation of the absorption of these EM waves by the wearer’s body. The SAR value must be in the RF exposure limit to ensure the wearer’s safety. However, for the frequency range of 400 MHz to 6 GHz, the ICNIRP and IEEE Std C95.1TM-2019 specifies the restriction in term of specific energy absorption (SA) of any 10-g cubic mass, where SA is restricted to $7.2 [0.05 + 0.95(\frac{t}{360})^{0.5}] \text{ kJ kg}^{-1}$ for the head and torso and $14.4 [0.025 + 0.975(\frac{t}{360})^{0.5}] \text{ kJ kg}^{-1}$ for limb exposure, where t

is the exposure interval in seconds. Note that for this specification, exposure from any pulse, group of pulses, or subgroup of pulses in a train, as well as from the total (sum) of exposures (including non-pulsed EMF), delivered in t seconds, must not exceed the limit (in order to ensure that the temperature thresholds are not exceeded) [41,42].

Table 5 illustrates that when the conventional antenna is worn on a child's arm (worst case), a small amount of reduction in maximum gain and directivity occurs for the lower frequency band. This means that some amount of power is consumed in the child's arm to increase the SAR level at the lower frequency band as compared to the upper frequency band. However, as shown in Figure 23, it is still in the SAR limit (<2 W/kg) because of the small amount of absorption of energy (demonstrated by the small reduction in gain and directivity at the lower resonance frequency (Table 5, 4th column). There is an increase in the maximum gain and directivity at the upper frequency band when the conventional antenna is worn on a child's arm. Thus, as shown in Figure 24, the SAR value at the higher frequency band is much lower than that at the lower frequency band.

Table 5. Maximum gain and directivity comparison between conventional antenna without a body and with a child's arm.

Parameter	Conventional Antenna without Body		Conventional Antenna Bent Around Arm of Radius 40 mm	
	f1 = 2.5	f2 = 5.196	f1 = 2.508	f2 = 5.224
Gain (dBi)	8.08	8.74	6.68	9.01
Directivity (dB)	8.39	9.01	7.7	9.29

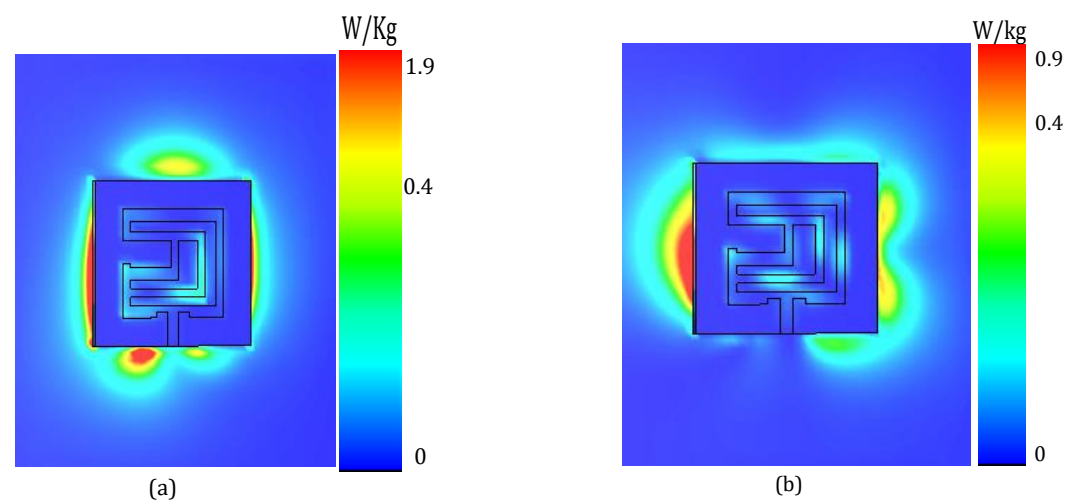


Figure 23. Conventional antenna SAR value on a flat body phantom at (a) 2.5 GHz and (b) 5.2 GHz.

The SAR values at both the resonance frequencies for the conventional antenna placed on a flat body phantom are given in Figure 22. These values are 0.332 W/kg and 0.234 W/kg averaged over 10 g of tissue for the lower and upper resonance bands, respectively. In case of the conventional antenna wrapped around the rounded body parts, the worst condition (child arm) among all bending conditions gives an SAR value of 1.89 W/kg and 0.462 W/kg taken over 10 g of tissue at 2.5 GHz and 5.2 GHz, respectively, as shown in Figure 23.

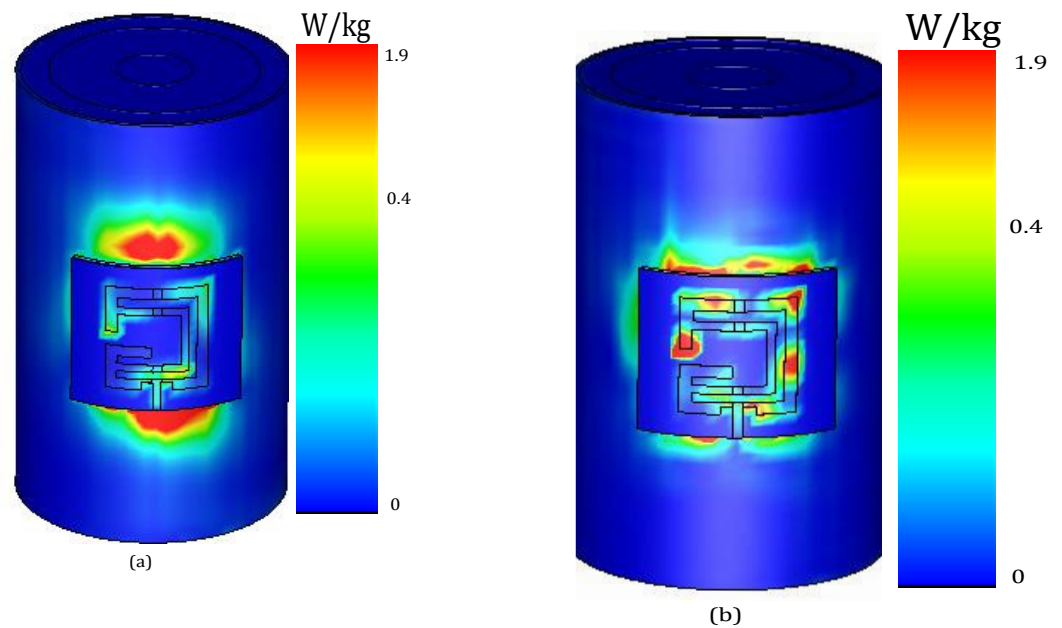


Figure 24. Conventional antenna's SAR value on a child's arm (worst case) of radius 40 mm at (a) 2.5 GHz and (b) 5.2 GHz.

The SAR analysis of the conventional dual band antenna shows that in all conditions, i.e., an antenna placed over a flat body phantom and an antenna wrapped around rounded body parts (when simulating a lower band of 2.5 GHz, a maximum allowable power of 5.7 mW and 53.8 mW was used for 1 g and 10 g, respectively; similarly, for the higher band of 5.2 GHz, a maximum allowable power of 10 mW and 90 mW was used for 1 g and 10 g, respectively), the obtained SAR value is within the RF exposure limit (<2 W/kg (European standard)) at both resonance frequencies. Hence, there is no need for EBG for the purpose of SAR. There are several reasons for the achieved lower SAR values. First, the proposed dual-band antenna has a full finite ground plane, which works as a reflector to protect the human body from radiation. Secondly, the radiation pattern of the patch antenna is perpendicular to the antenna plane. This is the reason that patch antenna is the best candidate among all types of antennas for wearable applications. Furthermore, as shown in Figures 20 and 21, when the designed antenna is mounted on the body, it radiates the minimum amount of side and back lobes towards the body. Based on these results, we consider that the proposed antenna can serve as an extremely useful component of many wearable applications, which cannot compromise on safety precautions due to their utilization in health critical systems.

4. Conclusions

In this paper, the design of a compact dual-band microstrip patch antenna operating at 2.5 and 5.2 GHz has been presented and analyzed for various critical parameters. With the help of two different EBG ground planes, improvement in the overall performance (in terms of directivity, gain, efficiency and other parameters) of the proposed dual band conventional ground plane antenna has been achieved. A comparison on the basis of the performance of the conventional antenna with two different EBG inspired antennas has been made, as given in Table IV. It is observed that EBG-inspired antennas achieve better performance compared to the antenna with a conventional ground plane. In addition, we tested the proposed dual band conventional ground plane antenna in various bending conditions. Based on our results, we conclude that the designed antenna remains tuned all the time, irrespective of the bending radii. Furthermore, we studied the proposed antenna design with respect to its contact with various human body parts (such as flat and rounded body parts) and performed a detailed SAR analysis. The corresponding results reveal that

at both the given resonance frequencies, the SAR value of the conventional antenna is well within the standard SAR limit (2 W/kg) prescribed by the European standards in both conditions when the antenna is placed over the flat body phantom (chest) or wrapped around the rounded body parts. Overall, we conclude that the proposed antenna design can be useful for a variety of applications including personal communications gadgets, equipment for combat and rescue operations, and health devices without compromising on the health of the wearer. An interesting future study is to ascertain the accuracy of the performance parameters by developing a wearable healthcare product to analyze the antenna performance practically.

Author Contributions: Conceptualization, F.F. and A.A.; formal analysis, F.F., A.A. and S.U.; funding acquisition, D.-Y.C. and A.A.; methodology, F.F., S.U., A.A. and D.-Y.C.; project administration, S.U. and D.-Y.C.; resources, A.A. and S.U.; software, F.F., S.U. and A.A.; supervision, S.U. and D.-Y.C.; validation, F.F., D.-Y.C. and S.U.; visualization, S.U., F.F. and A.A.; writing—original draft, F.F., S.U. and A.A.; writing—review and editing, D.-Y.C. and S.U. All authors have read and agreed to the published version of the manuscript.

Funding: This research was supported by the Basic Science Research Program through the National Research Foundation of Korea (NRF) funded by the Ministry of Education (2022R111A3064544).

Institutional Review Board Statement: Not applicable.

Informed Consent Statement: Not applicable.

Data Availability Statement: Not applicable.

Conflicts of Interest: The authors declare no conflict of interest.

References

1. Xiangfang, R.; Lei, S.; Miaomiao, L.; Xiying, Z.; Han, C. Research and sustainable design of wearable sensor for clothing based on body area network. *Cogn. Comput. Syst.* **2021**, *3*, 206–220. [\[CrossRef\]](#)
2. Ali, S.M.; Sovuthy, C.; Imran, M.A.; Socheatra, S.; Abbasi, Q.H.; Abidin, Z.Z. Recent advances of wearable antennas in materials, fabrication methods, designs, and their applications: State-of-the-art. *Micromachines* **2020**, *11*, 888. [\[CrossRef\]](#) [\[PubMed\]](#)
3. Elsheikh, D.M.; Abdallah, E.A. Different feeding techniques of microstrip patch antennas with spiral defected ground structure for size reduction and ultra-wide band operation. *J. Electromagn. Anal. Appl.* **2012**, *4*, 410–418. [\[CrossRef\]](#)
4. Fallahpour, M.; Zoughi, R. Antenna miniaturization techniques: A review of topology-and material-based methods. *IEEE Antennas Propag. Mag.* **2017**, *60*, 38–50. [\[CrossRef\]](#)
5. Ahmad, A.; Arshad, F.; Naqvi, S.I.; Amin, Y.; Tenhunen, H.; Loo, J. Flexible and compact spiral-shaped frequency reconfigurable antenna for wireless applications. *IETE J. Res.* **2020**, *66*, 22–29. [\[CrossRef\]](#)
6. Mahfuz, M.H.; Islam, M.R.; Park, C.W.; Elsheikh, E.A.; Suliman, F.; Habaebi, M.H.; Malek, N.A.; Sakib, N. Wearable Textile Patch Antenna: Challenges and Future Directions. *IEEE Access* **2022**, *10*, 38406–38427. [\[CrossRef\]](#)
7. Ali, U.; Ullah, S.; Khan, J.; Shafi, M.; Kamal, B.; Basir, A.; Flint, J.A.; Seager, R.D. Design and SAR analysis of wearable antenna on various parts of human body, using conventional and artificial ground planes. *J. Electr. Eng. Technol.* **2017**, *12*, 317–328. [\[CrossRef\]](#)
8. Augustine, R.; Alves, T.; Sarrebourg, T.; Poussot, B.; Mathew, K.; Laheurte, J.M. Polymeric ferrite sheets for SAR reduction of wearable antennas. *Electron. Lett.* **2010**, *46*, 197. [\[CrossRef\]](#)
9. Augustine, R.; Alves, T.; Zhadobov, M.; Poussot, B.; Sarrebourg, T.; Sauleau, R.; Thomas, M.K.; Laheurte, J.M. SAR reduction of wearable antennas using polymeric ferrite sheets. In Proceedings of the Fourth European Conference on Antennas and Propagation, Barcelona, Spain, 12–16 April 2010; pp. 1–3.
10. Jensen, M.A.; Rahmat-Samii, Y. EM interaction of handset antennas and a human in personal communications. *Proc. IEEE* **1995**, *83*, 7–17. [\[CrossRef\]](#)
11. Li, H.; Tsiaras, A.; Lau, B.K. Analysis and estimation of MIMO-SAR for multi-antenna mobile handsets. *IEEE Trans. Antennas Propag.* **2017**, *65*, 1522–1527. [\[CrossRef\]](#)
12. Ramachandran, T.; Faruque, M.R.I.; Islam, M.T. Specific absorption rate reduction for sub-6 frequency range using polarization dependent metamaterial with high effective medium ratio. *Sci. Rep.* **2022**, *12*, 1–18. [\[CrossRef\]](#) [\[PubMed\]](#)
13. Ramachandran, T.; Faruque, M.R.I.; Ahamed, E.; Abdullah, S. Specific absorption rate reduction of multi split square ring metamaterial for L-and S-band application. *Results Phys.* **2019**, *15*, 102668. [\[CrossRef\]](#)
14. Mallik, A.; Kundu, S.; Goni, M.O. Gain and SAR improvement of a conventional patch antenna using a novel Pi-shaped DNG metamaterial. In Proceedings of the 2013 International Conference on Electrical Information and Communication Technology (EICT), Khulna, Bangladesh, 13–15 February 2014; pp. 1–6.

15. Janapala, D.K.; Nesasudha, M.; Neebha, T.M.; Kumar, R. Specific absorption rate reduction using metasurface unit cell for flexible polydimethylsiloxane antenna for 2.4 GHz wearable applications. *Int. J. RF Microw.-Comput.-Aided Eng.* **2019**, *29*, e21835. [[CrossRef](#)]
16. Islam, M.T.; Faruque, M.R.I.; Misran, N. Reduction of specific absorption rate (SAR) in the human head with ferrite material and metamaterial. *Prog. Electromagn. Res. C* **2009**, *9*, 47–58. [[CrossRef](#)]
17. Potey, P.M.; Tuckley, K. Design of wearable textile antenna for low back radiation. *J. Electromagn. Waves Appl.* **2020**, *34*, 235–245. [[CrossRef](#)]
18. Song, L.; Rahmat-Samii, Y. A systematic investigation of rectangular patch antenna bending effects for wearable applications. *IEEE Trans. Antennas Propag.* **2018**, *66*, 2219–2228. [[CrossRef](#)]
19. El May, W.; Sfar, I.; Ribero, J.M.; Osman, L. A millimeter-wave textile antenna loaded with EBG structures for 5G and IoT applications. In Proceedings of the 2019 IEEE 19th Mediterranean Microwave Symposium (MMS), Hammamet, Tunisia, 31 October–2 November 2019; pp. 1–4.
20. Harine, G.; Abirami, S.; Harini, B.; Florence, S.E.; Subramaniam, I. Design and Analysis of Novel EBG/AMC Unit Cell. In Proceedings of the 2019 5th International Conference on Advanced Computing & Communication Systems (ICACCS), Coimbatore, India, 15–16 March 2019; pp. 684–688.
21. Rano, D.; Hashmi, M. Extremely compact EBG-backed antenna for smartwatch applications in medical body area network. *IET Microwaves, Antennas Propag.* **2019**, *13*, 1031–1040. [[CrossRef](#)]
22. Zu, H.; Wu, B.; Yang, P.; Li, W.; Liu, J. Wideband and High-Gain Wearable Antenna Array with Specific Absorption Rate Suppression. *Electronics* **2021**, *10*, 2056. [[CrossRef](#)]
23. Ahmad, A.; Choi, D.y.; Ullah, S. A compact two elements MIMO antenna for 5G communication. *Sci. Rep.* **2022**, *12*, 1–8. [[CrossRef](#)]
24. Chen, X.; Zhang, S.; Li, Q. A review of mutual coupling in MIMO systems. *IEEE Access* **2018**, *6*, 24706–24719. [[CrossRef](#)]
25. Mohamadzade, B.; Lalbakhsh, A.; Simorangkir, R.B.; Rezaee, A.; Hashmi, R.M. Mutual coupling reduction in microstrip array antenna by employing cut side patches and EBG structures. *Progress Electromagn. Res. M* **2020**, *89*, 179–187. [[CrossRef](#)]
26. Khan, A.; Bashir, S.; Ghafoor, S.; Qureshi, K.K. Mutual coupling reduction using ground stub and EBG in a compact wideband MIMO-antenna. *IEEE Access* **2021**, *9*, 40972–40979. [[CrossRef](#)]
27. Acharjee, J.; Mandal, K.; Mandal, S.K. Reduction of mutual coupling and cross-polarization of a MIMO/diversity antenna using a string of H-shaped DGS. *AEU-Int. J. Electron. Commun.* **2018**, *97*, 110–119. [[CrossRef](#)]
28. Trivedi, K.; Pujara, D. Mutual coupling reduction using defected ground structure in UWB DRA array for MIMO application. In Proceedings of the 2020 IEEE International Symposium on Antennas and Propagation and North American Radio Science Meeting, Montreal, QC, Canada, 5–10 July 2020; pp. 1879–1880.
29. Ahmad, U.; Ullah, S.; Rafique, U.; Choi, D.Y.; Ullah, R.; Kamal, B.; Ahmad, A. MIMO Antenna System With Pattern Diversity for Sub-6 GHz Mobile Phone Applications. *IEEE Access* **2021**, *9*, 149240–149249. [[CrossRef](#)]
30. Hossain, M.; Faruque, M.R.I.; Islam, M.T. Analysis on the effect of the distances and inclination angles between human head and mobile phone on SAR. *Prog. Biophys. Mol. Biol.* **2015**, *119*, 103–110. [[CrossRef](#)]
31. Yalduz, H.; Tabaru, T.E.; Kilic, V.T.; Turkmen, M. Design and analysis of low profile and low SAR full-textile UWB wearable antenna with metamaterial for WBAN applications. *AEU-Int. J. Electron. Commun.* **2020**, *126*, 153465. [[CrossRef](#)]
32. Abbas, S.M.; Ranga, Y.; Esselle, K.P. Sensitivity of a wearable printed antenna with a full ground plane in close proximity to human arm. In Proceedings of the 2015 9th European Conference on Antennas and Propagation (EuCAP), Lisbon, Portugal, 12–17 April 2015; pp. 1–4.
33. Elias, N.; Samsuri, N.; Rahim, M. Analytical study of energy absorption in human body due to bendable behaviour of textile antenna. In *Theory and Applications of Applied Electromagnetics*; Springer: Berlin/Heidelberg, Germany, 2015; pp. 329–337.
34. Pandimadevi, M.; Tamilselvi, R.; Parisa Beham, M. Design and simulation of flexible jute antenna with performance validation on bending and soaking conditions. *Text. Res. J.* **2021**, *91*, 219–231. [[CrossRef](#)]
35. Balanis, C.A. *Antenna Theory: Analysis and Design*; John Wiley & Sons: Hoboken, NJ, USA, 2015.
36. Ahmad, A.; Faisal, F.; Khan, S.; Ullah, S.; Ali, U. Performance analysis of a wearable and dual band planar antenna using a mushroom-like electromagnetic bandgap (EBG) ground plane. In Proceedings of the 2015 International Conference on Open Source Systems & Technologies (ICOSST), Lahore, Pakistan, 17–19 December 2015; pp. 24–29.
37. Faisal, F.; Ahmad, A.; Ali, U.; Ullah, S.; Ullah, K. Performance analysis of a 2.4 GHz planar antenna using different types of wearable artificial ground planes. In Proceedings of the 2015 12th International Conference on High-capacity Optical Networks and Enabling/Emerging Technologies (HONET), Islamabad, Pakistan, 21–23 December 2015; pp. 1–5.
38. Saraereh, O.A. Microstrip wearable dual-band antenna design for ON body wireless communications. In Proceedings of the 2019 IEEE 4th International Conference on Computer and Communication Systems (ICCCS), Singapore, 23–25 February 2019; pp. 585–589.
39. Hasan, M.; Faruque, M.R.I.; Islam, M.T. Dual band metamaterial antenna for LTE/bluetooth/WiMAX system. *Sci. Rep.* **2018**, *8*, 1–17. [[CrossRef](#)]
40. Sankaralingam, S.; Gupta, B. Development of textile antennas for body wearable applications and investigations on their performance under bent conditions. *Prog. Electromagn. Res. B* **2010**, *22*, 53–71. [[CrossRef](#)]

41. International Commission on Non-Ionizing Radiation Protection (ICNIRP). Guidelines for limiting exposure to electromagnetic fields (100 kHz to 300 GHz). *Health Phys.* **2020**, *118*, 483–524. [[CrossRef](#)]
42. Bailey, W.H.; Bodemann, R.; Bushberg, J.; Chou, C.K.; Cleveland, R.; Faraone, A.; Foster, K.R.; Gettman, K.E.; Graf, K.; Harrington, T.; et al. Synopsis of IEEE Std C95. 1TM-2019 “IEEE Standard for Safety Levels With Respect to Human Exposure to Electric, Magnetic, and Electromagnetic Fields, 0 Hz to 300 GHz”. *IEEE Access* **2019**, *7*, 171346–171356. [[CrossRef](#)]